Pergamon

Journal of Structural Geology, Vol. 16, No. 4, pp. 571 to 584, 1994

0191-8141/94 $06.00+0.00

Kinematics of fault-related folding in a duplex, Lost River Range, Idaho, U.S.A.

CHRISTOPHER A. HEDLUND* and DAVID J. ANASTASIO

Department of Earth and Environmental Sciences, Lehigh University, Bethlehem, PA 18015, U.S.A.

and

DONALD M. FISHER

Department of Geosciences, Pennsylvania State University, University Park, PA 16802, U.S.A.

(*Received* 20 *December* 1992; *accepted in revised form* 10 *September* 1993)

Abstract—The Doublespring duplex, located in the Lost River Range of Idaho, is a Sevier age fault-related fold complex in massive limestones of the Upper Mississippian Scott Peak Formation. Folds within the duplex closely resemble fault-bend fold geometries, with open interlimb angles and low-angle bed cut-offs. Narrow, widely spaced, bedding-parallel shear zones with well-developed pressure solution cleavage alternate with massive, relatively undeformed layers on fold limbs. Shear zones are developed only on the limbs of anticlines, and have similar but unique morphologies in each of three different folds. Incremental strain histories reconstructed from antitaxial fibrous overgrowths and veins within the shear zones constrain the kinematics of folding. Shear zones experienced distributed bedding-parallel simple shear (flexural flow) towards pins near axial surfaces, while adjacent massive layers experienced rotation through an externally fixed extension direction. The absence of footwall synclines and morphological differences in shear zones from adjacent folds suggest that faulting preceded folding. Kinematic histories of folds that have experienced different translational histories are identical, and are not compatible with strain histories predicted from previous kinematic models of fault-bend folding. Shear zone development and fiber growth is instead interpreted to have occurred during low amplitude fixed-hinge buckling in response to initial resistance to translation of the thrust sheet. Fault-bend folding with mobile axial surfaces occurred with translation of the thrust sheets once the initial resistance to translation was overcome and resulted in no penetrative strain.

INTRODUCTION

THE complex relationship between faulting and folding in foreland fold–thrust belts has intrigued structural geologists for decades (e.g. Willis 1893, Rich 1934, Boyer 1986). Currently, fault-related folds are generally recognized to be either: (1) fault-bend folds which form in response to displacement on a non-planar or stepped fault surface (Rich 1934, Suppe 1983); (2) fault-propagation folds which accommodate shortening above a propagating thrust ramp (Suppe & Medwedeff 1984, 1990, Mitra 1990); or (3) décollement folds which form above a bedding-parallel thrust segment (Dahlstrom 1970, Jamison 1987). The geometry and kinematics of fault-related folding are intimately related; fold geometry depends in part on the orientation and distribution of shear during folding, and the details of fold kinematics are affected by the geometry of the fault. Kinematic models predicting the geometric evolution of fault-related folds (Sanderson 1982, Suppe 1983, Suppe & Medwedeff 1984) closely simulate the geometry of natural structures and provide the basis for geometric reconstructions of fold–thrust structures.

Although the geometries of natural fault-related folds have been studied extensively, only recently have empirical studies begun to place constraints on the kinematic evolution of natural fault-related folds. Beutner *et al.* (1988) interpreted incremental strain data from the Hamburg sequence to represent folding by vertical simple shear at axial surfaces fixed with respect to a footwall ramp. More recently, Fischer *et al.* (1992) and Fisher & Anastasio (1994) have presented evidence for a fixed-hinge buckling origin for asymmetric fault-related folds in the Appalachian and Sevier thrust belts based on the distribution of structural fabrics and incremental strain histories. The importance of kinematics in the interpretation, evaluation and reconstruction of geologic structures is widely recognized (e.g. Geiser 1988). This paper presents results from a kinematic analysis of fault-related folds in a duplex using incremental strain analysis of syntectonic fibers in pressure shadows and veins. These results give insights into the partitioning of fold mechanisms in a layered sequence and provide constraints on the timing and distribution of deformation during fault-related folding.

KINEMATIC MODELS OF FAULT-RELATED FOLDING

Models of fault-related folding predict specific distributions of strain associated with folding and provide a basis for comparison to natural structures. Fault-bend folding models assume deformation occurs by bedding-parallel shear exclusively such that bed thickness and length is always conserved (Sanderson 1982, Suppe

*Current address: Department of Earth Resources, Colorado State University, Fort Collins, CO 80523, U.S.A.

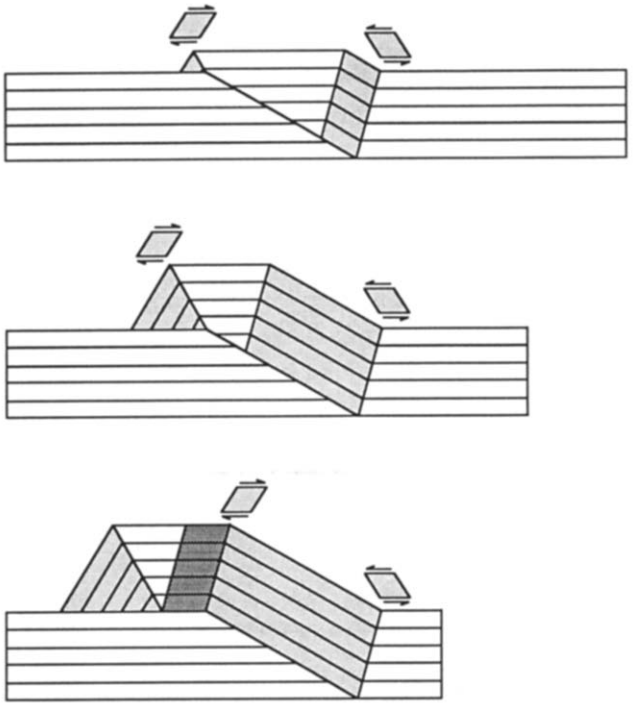

Fig. 1. Distribution of bedding-parallel simple shear associated with parallel fault-bend folding (after Suppe 1983). Sense of shear at different axial surfaces is indicated by parallelograms and arrows. Unsheared domains are shown in white, once sheared domains in light grey, and twice sheared domains in dark grey. Note the reversal of shear direction at the top of the footwall ramp.

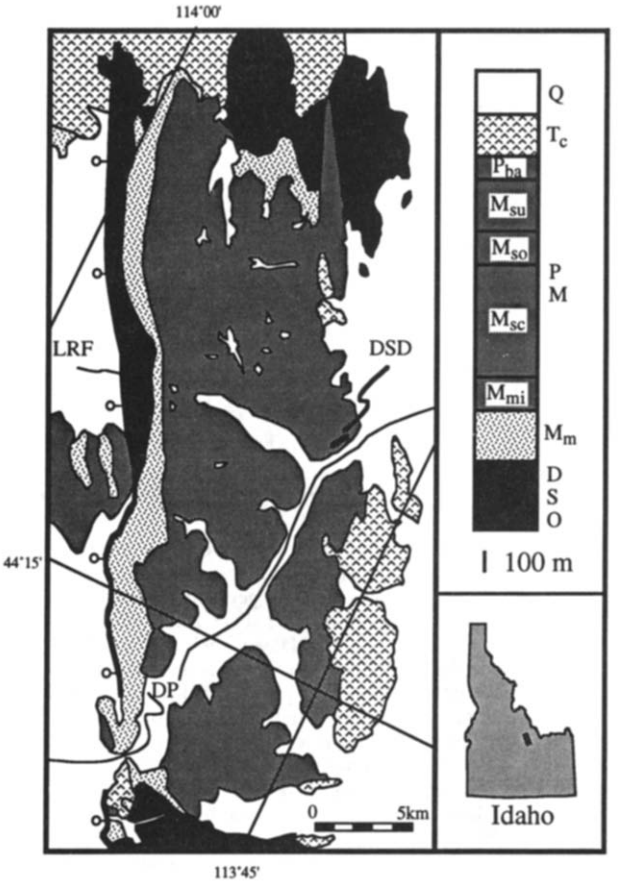

Fig. 2. Simplified geologic map of the northern Lost River Range, Idaho, indicating the location of the Doublespring duplex (after Mapel *et al.* 1965). LRF = Lost River Fault, DSD = Doublespring duplex, DP = Doublespring Pass Road. Stratigraphic units: Tcv = Challis Volcanics, Pba = Bluebird Mountain and Arco Hills Formations, Msu = Surrett Canyon Formation, Mso = South Creek Formation, Msc = Scott Peak Formation, Mmi = Middle Canyon Formation, Mm = McGowan Creek Formation, DSO = undifferentiated Lower Paleozoic.

1983). Deformation in these models occurs only at axial surfaces fixed at fault bends. Axial surfaces migrate and the distribution of simple shear changes through the evolution of the structure as displacement increases (Fig. 1). Specific predictions of these models include a shear reversal at the top of the ramp and the existence of a wedge of material above the lower hanging wall cutoff that has not experienced any fold-related shear (Fig. 1). For simple ramp geometries, the magnitude of bedding-parallel shear strain due to folding is related the dip of the thrust ramp (Sanderson 1982).

Because décollement or buckle folds form independently of a rigid footwall they can be highly variable, and no single unique model simulates the wide variety of possible geometries for these structures (e.g. Laubscher 1976, Jamison 1987, Mitra 1992). The distribution of shear associated with buckle folding depends on the location of pin lines (Woodward *et al.* 1989). Décollement folds originating in response to a buckling instability with pins fixed at axial surfaces result in a reversal of shear direction on different limbs of the fold (e.g. Fischer *et al.* 1992, Fisher & Anastasio 1994). The kinematics and distribution of simple shear associated with fault-propagation folding were recently reviewed in Suppe & Medwedeff (1990) and Fischer *et al.* (1992).

THE DOUBLESPRING DUPLEX

Geologic setting

The structure considered in this study is located near Doublespring, in the northern Lost River Range (Fig. 2). The Lost River Range is the westernmost in a series of NNW–SSE-trending ranges in the part of the Basin and Range province north of the Snake River Plain in south-central Idaho, U.S.A. The range is bounded to the west by the seismically active Lost River Fault (Crone & Haller 1991, and references therein), and to both the east and west by structural basins formed by Miocene-Holocene extension (Ross 1947, Baldwin 1951, Mapel *et al.* 1965). The northern Lost River Range (Fig. 2) is a first-order synclinorium exposing a thick Upper Mississippian–Lower Pennsylvanian carbonate bank sequence (Mamet *et al.* 1971, Rose 1977, Skipp *et al.* 1979). The McGowan Creek Formation, a tapered wedge of Lower Mississippian flysch derived from the Antler highlands to the west, separates the Upper Paleozoic carbonate shelf sequence from the underlying Lower Paleozoic mixed carbonate–clastic sequence (Mapel *et al.* 1965, Skipp *et al.* 1979) and served as a regional décollement above which numerous E-vergent, NNE–SSW-trending fault-related folds formed in the Upper Paleozoic sequence during the Sevier Orogeny (Fisher & Anastasio 1994).

The structure exposed at Doublespring occurs in the Scott Peak Formation, a 700 m thick limestone unit consisting of massive biomicrite beds with thin chert nodule-rich beds spaced from 1 to 15 m. The Doublespring structure formed above a local décollement within the Scott Peak Formation approximately 325 m above the regional décollement in the McGowan Creek Formation.

Geometry

The Doublespring structure consists of a folded sequence of massive limestone beds on the homoclinally dipping (25° towards N70°E) flank of a larger-order anticline (Figs. 3a & b). Stratigraphic cutoff geometries and axial surface relationships constrain the geometry of the underlying imbricate thrusts, and indicate that folds are closely related to these faults. These constraints provide the basis for a line-length and area-balanced cross-section of the Doublespring structure (Fig. 5). The Doublespring structure is interpreted to be a hinterland dipping duplex (Boyer & Elliott 1982) where two imbricate thrusts converge at a leading branch line to form a single horse. A minimum of 50 m of shortening is accommodated by displacement on this fault system.

Three anticlines in the Doublespring duplex (Figs. 3b and 5) are the focus of the kinematic analysis, and are henceforth referred to as the upper, middle and lower folds. These folds are curved (rather than kinked), parallel and cylindrical in geometry (Fig. 6), with open interlimb angles ranging from 130° to 145°. The upper fold is a leading-edge fold that has experienced little translation such that the lower hanging wall cutoffs have not been translated to the upper footwall cutoffs, and is located at the top of the footwall ramp. In the middle fold the lower hanging wall cutoffs have been translated approximately 25 m beyond the upper footwall cutoffs such that the fold is located on a footwall flat a relatively long distance away from the corresponding footwall ramp. Antithetic reverse faults with minor displacement are formed at the leading edges of the upper and middle folds (Figs. 3 and 5). While the relationship of the lower fold to an underlying thrust is less constrained due to a lack of exposure, depth-to-detachment considerations, axial surface orientations, and the continuation of the forelimb at regional orientation indicate that it is likely located at the top of an underlying footwall ramp. Alternatively, the lower fold may be a décollement fold. Thus each of the three folds has experienced a different translational history and structural evolution, and rocks within these folds would be expected to have recorded different kinematic histories.

Bedding-parallel shear zones

A prominent feature in folds of the Doublespring duplex is the presence of relatively thin (5 cm–1 m thick), widely spaced, recessively weathering, bedding-parallel layers in the otherwise massive sequence of limestone. In contrast with the adjacent relatively undeformed layers, these layers are characterized by a penetrative pressure solution fabric spaced on the order of millimeters, refracted cleavage orientation, high finite strains, en échelon extensional vein arrays and layer-parallel shear surfaces (Fig. 7). These layers are interpreted to be bedding-parallel brittle–ductile shear zones (Ramsay & Graham 1970). The shear zones are developed only on fold limbs, and grade laterally into massive layers where little fold-related strain has occurred (in flat segments above the décollement and at pinned fold hinges). Shear zones in the Doublespring structure are thus interpreted to have formed from an initially massive protolith as a consequence of deformation associated with folding. The termination of shear zones near fold hinges generally occurs abruptly over less than 2–3 m, suggesting a high strain gradient.

Although shear zones in each of the folds have many common features, shear zones from each fold have characteristic features that are unique (Fig. 7). Shear zones in the upper fold have sharply defined bedding-parallel boundaries, range in thickness from 5 to 10 cm, and have an anastamosing bedding-parallel fabric consisting of a penetrative pressure solution cleavage with locally abundant cleavage-parallel extensional veins (Fig. 7). Relatively high-amplitude asperities (up to half the shear zone thickness) exist in the shear zone bounding surfaces of the upper fold. Shear zones in the middle fold are characterized by sharply defined bedding-parallel boundaries, cleavage inclined at a moderate angle from bedding, and locally well-developed en échelon vein arrays and bedding-parallel faults (Fig. 7). The shear zone in the lower fold is characterized by diffuse boundaries, an anastamosing cleavage orientation ranging from moderately inclined from bedding to nearly bedding-parallel (Fig. 7), and locally developed bedding-parallel shear surfaces and en échelon extensional vein arrays. Cleavage in the middle and lower folds dips away from the hinge to form a convergent fan. En échelon vein arrays generally indicate shear toward the fold hinge, although some cleavage-parallel veins also exist. En échelon veins and shear zone-bounding faults cross-cut cleavage and show no sign of internal pressure solution fabric development, suggesting a late-stage origin for these features.

The relatively thick layers between shear zones are massive and undeformed in comparison with the shear zones. A weakly developed disjunctive cleavage (domains spaced on the order of tens of centimeters) is typically oriented at a steep angle to bedding in the massive layers forming a convergent fan, although isolated stylolites occur at almost any orientation. Extensional veins in massive layers are uncommon and show no systematic orientation.

The development of highly strained shear zones between relatively undeformed layers indicates inhomogeneous deformation where deformation is initially localized by heterogeneities in an otherwise isotropic material (Ramsay 1982). Shear zones in all three folds form in a bed with relatively abundant black chert

nodules measuring approximately 10–20 cm in diameter, which may have acted as stress concentrators that could have initially localized deformation. The presence of relatively insoluble residue (i.e. phyllosilicates and Fe-oxides) in cleavage domains, fibrous overgrowths in pressure shadows, and both fibrous and sparry extensional veins indicate that pressure solution was an important deformation mechanism within the shear zones. Deformation may have also been localized in this layer because of a slightly higher detrital content or a finer matrix grain size, both of which would have enhanced the effectiveness of pressure solution (Rutter 1976, Marshak & Engelder 1985). Once deformation commenced in the incipient shear zones, chemical and geometric strain softening by concentration and alignment of phyllosilicates allowed the accumulation of large amounts of strain within the shear zones while adjacent rock experienced relatively little deformation.

INCREMENTAL STRAIN ANALYSIS

Displacement-controlled fibrous mineral overgrowths provide a continuous record of the incremental extension direction during deformation by mass transfer, and form the basis for a method to reconstruct incremental strain histories by measuring fiber trajectories (Elliott 1972, Durney & Ramsay 1973). The effectiveness of incremental strain histories recorded by displacement-controlled fibers in constraining the kinematics of deformation associated with cleavage development (Fisher 1990), folding (Wickham & Anthony 1977, Beutner & Diegel 1985, Beutner *et al.* 1988, Fisher & Anastasio 1994) and accretionary prism evolution (Sample & Fisher 1986, Fisher & Byrne 1992, Clark *et al.* 1993) has been demonstrated. Fibrous overgrowths in pressure shadows (Figs. 4a–c) and fibrous extensional veins (Fig. 4d) are common in approximately 50% of the samples from shear zones in the Doublespring structure. In contrast, only two isolated samples (less than 5%) from the massive layers contain fibrous overgrowths.

Fibers in pressure shadows are most commonly composed of calcite on host grains of quartz replaced bioclasts (Figs. 4a & b), although quartz fibers on framboidal pyrite also occur (Fig. 4c). R_f/ϕ analysis of crinoid ossicles in samples from shear zones indicates that bioclasts behaved as rigid porphyroclasts and have experienced little or no internal deformation. Subspherical quartz and pyrite host grains, pressure shadow shapes that approximate host grain boundary shapes, and curved fibers that are not always normal to growth interfaces indicate that fiber growth in pressure shadows was displacement-controlled (Ramsay & Huber 1987).

Several observations indicate that fiber growth in pressure shadows was antitaxial (pyrite-type of Ramsay & Huber 1983), occurring at the porphyroclast surface. Where the mineralogy of the fibers differs from that of the host grain, as in the Doublespring structure, fiber growth is generally antitaxial (Durney & Ramsay 1973). Calcite fibers in optical continuity with matrix calcite also indicate antitaxial growth (Durney & Ramsay 1973).

Straight displacement-controlled fiber trajectories indicate a coaxial incremental strain history, while curved fiber trajectories may result from either a non-coaxial incremental strain history (i.e. rotation of the incremental extension direction relative to the finite extension direction), bending of initially straight fibers, or a combination of these factors. Approximately 25% of the fibers in the Doublespring duplex shear zones have been obviously deformed, as indicated by twinned or recrystallized calcite fibers, quartz fibers with undulose extinction, or fiber bundles that taper away from the porphyroclast. The majority of the curved fibers, however, are relatively undeformed, as indicated by optically continuous and untwinned fibers with fiber bundle shapes that approximately parallel host grain boundaries (Durney & Ramsay 1973, Ramsay & Huber 1983, 1987, Fisher & Byrne 1992). The curvature of these fibers is interpreted to be primary and a result of non-coaxial incremental strain histories. Only these relatively undeformed fibers were analysed in this study. To minimize the effects of porphyroclast matrix coupling, only fibers in pressure shadows adjacent to sub-spherical host grains were measured, and only the central fiber was measured from each pressure shadow.

Methods

Two types of methods exist for the reconstruction of incremental strain histories from syntectonic displacement-controlled fibers, those that apply an unstraining routine to correct for passive deformation of fibers (Ellis 1986, Ramsay & Huber 1987), and those that do not (Durney & Ramsay 1973, Wickham 1973). Durney & Ramsay's (1973) method was used in this study, resulting in calculated incremental strain histories that are a more direct representation of the fiber shape (Fisher & Byrne 1992). To facilitate incremental strain history reconstruction, curved fiber trajectories can be approximated by a series of straight fiber segments representing coaxial increments separated by rigid rotations (Elliott 1972). The orientation of each segment relative to a reference direction (i.e. cleavage, bedding or horizontal) records the orientation of the incremental extension direction, and the segment length normalized to the initial length (host grain radius plus the length of previous fiber increments measured in the extension direction) represents the magnitude of incremental elongation. Incremental strain histories are measured from fibrous veins in much the same way as from fibrous overgrowths, with the exception that elongation magnitudes are scaled to the width of wall rock domains between individual veins rather than to the host grain diameter.

In this study, incremental strain histories have been reconstructed for fibers viewed in both cleavage-parallel (Z) and fold axis-normal (Y) sections. Z sections were viewed looking down onto the cleavage plane, and Y

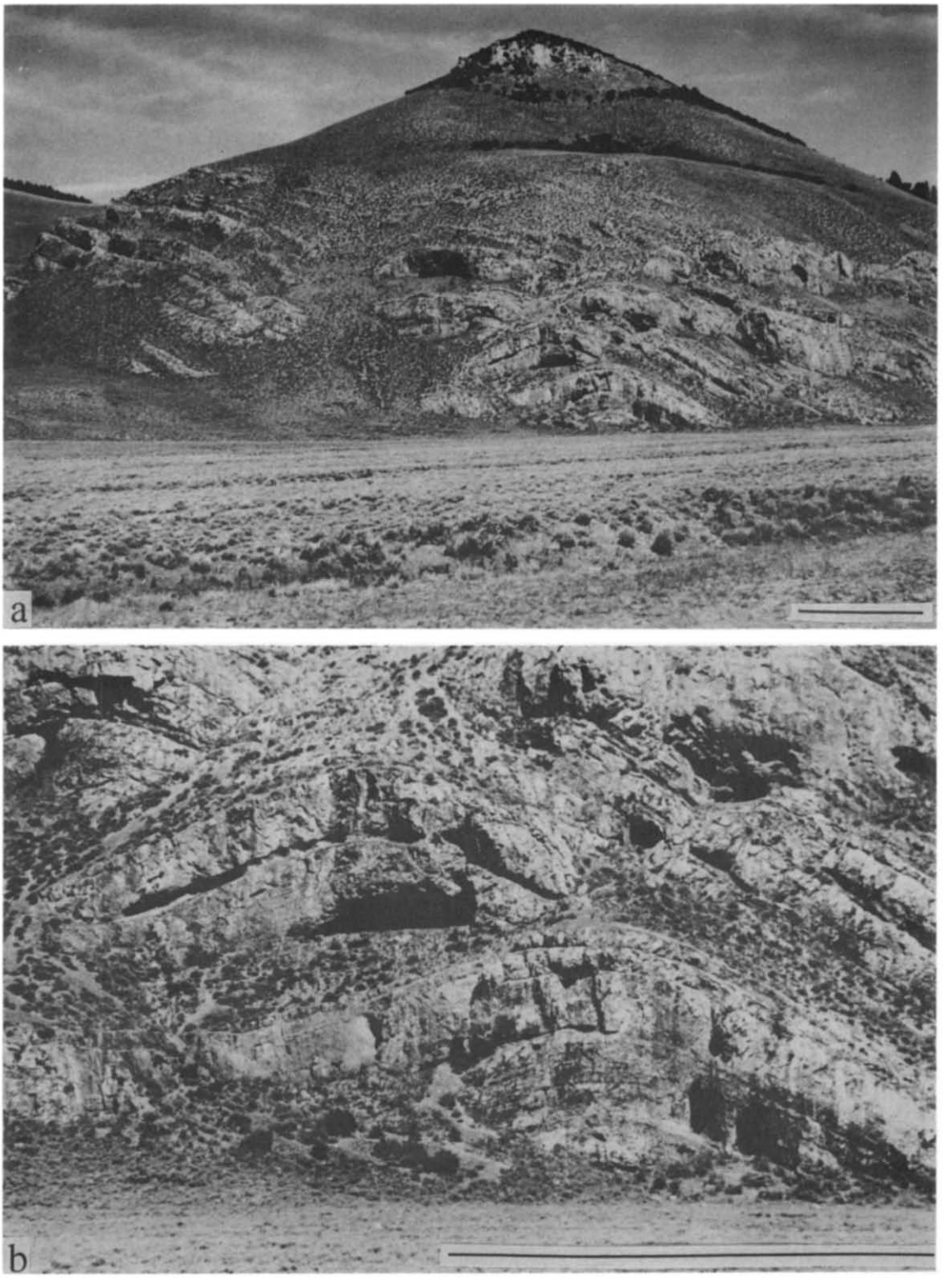

Fig. 3. (a) Photograph of the Doublespring duplex. View is parallel to the fold axis, towards N20°W. (b) Close up photograph of the three anticlinal folds in the Doublespring duplex. View is parallel to the fold axis, towards N20°W. Scale bars 25 m.

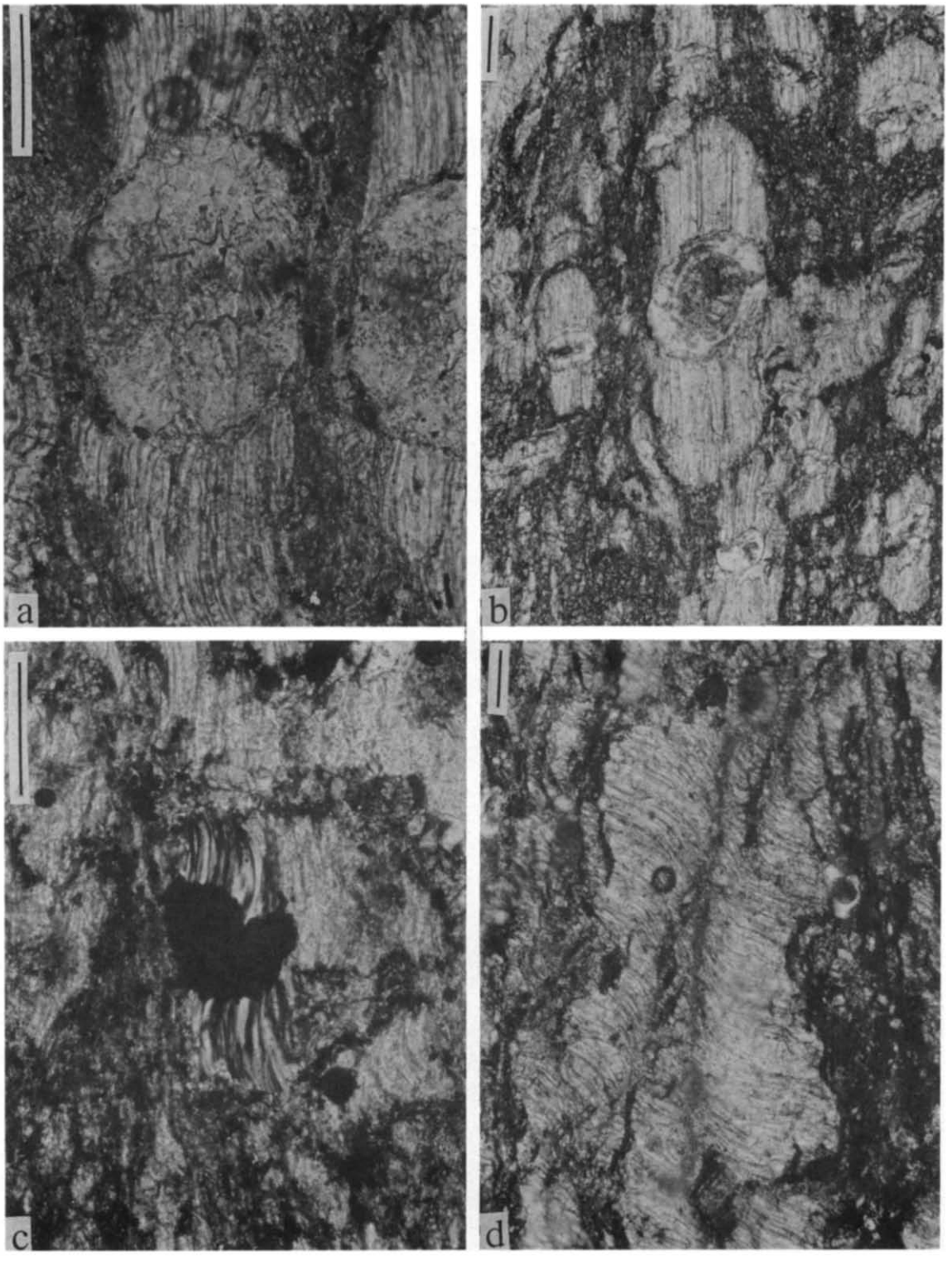

Fig. 4. Photomicrographs of pressure shadows and veins from samples cut perpendicular (a, c & d) to the bedding–cleavage intersection with the cleavage trace parallel to the long axis of the photograph. Photomicrograph of a pressure shadow in a sample cut parallel to cleavage with the long axis of the photograph parallel to the dip direction. (a) Quartz-replaced crinoid ossicle with antitaxial calcite fibers showing non-coaxial strain histories; (b) quartz-replaced crinoid ossicle with antitaxial calcite fibers showing coaxial strain histories; (c) antitaxial quartz fibers on framboidal pyrite showing non-coaxial strain histories; and (d) antitaxial extensional vein filled with fibrous calcite. Cleavage is parallel to the long axis of the photograph in all cases. Scale bars 200 μm.

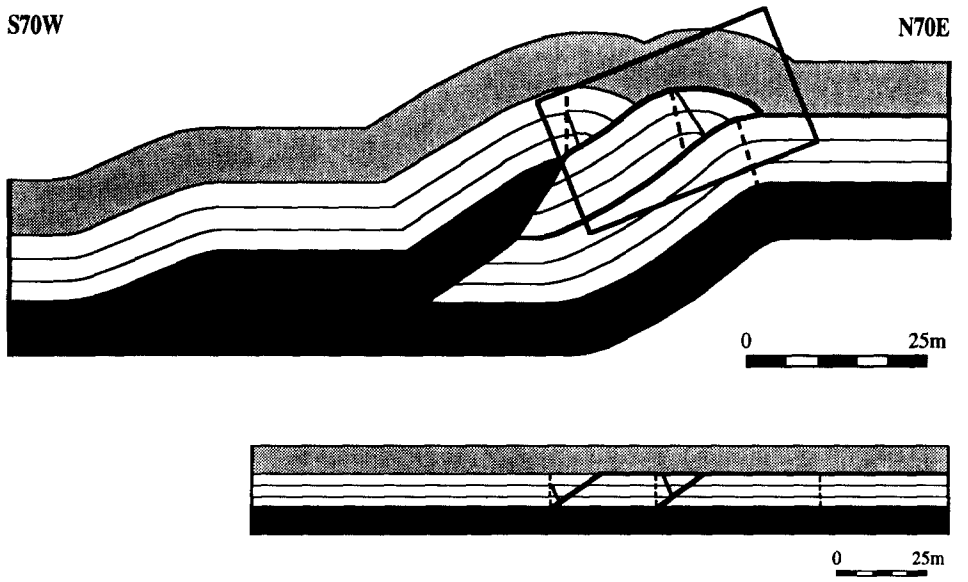

Fig. 5. Bed-length and area-balanced deformed- and restored-state cross-sections of Doublespring duplex. A regional dip of 25° towards N70E has been removed. Restored section is displayed at half-scale of the deformed section. Present and restored locations of fold axial planes are shown as dashed lines. Box indicates area of sketch shown in Fig. 10.

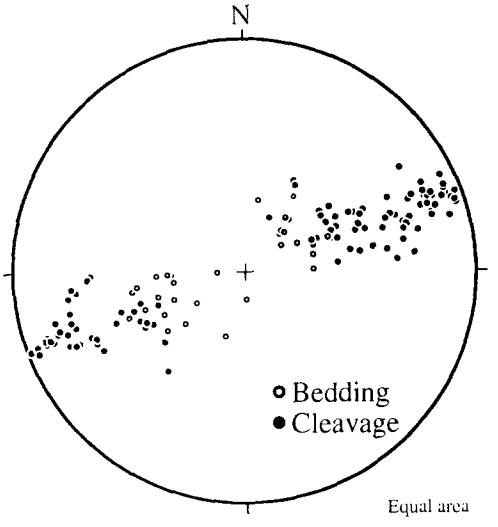

Fig. 6. Equal-area stereoplot of poles to bedding (open circles) and cleavage (solid circles) in the Doublespring duplex. A narrow distribution of orientations show that folds in the Doublespring duplex are approximately cylindrical in geometry.

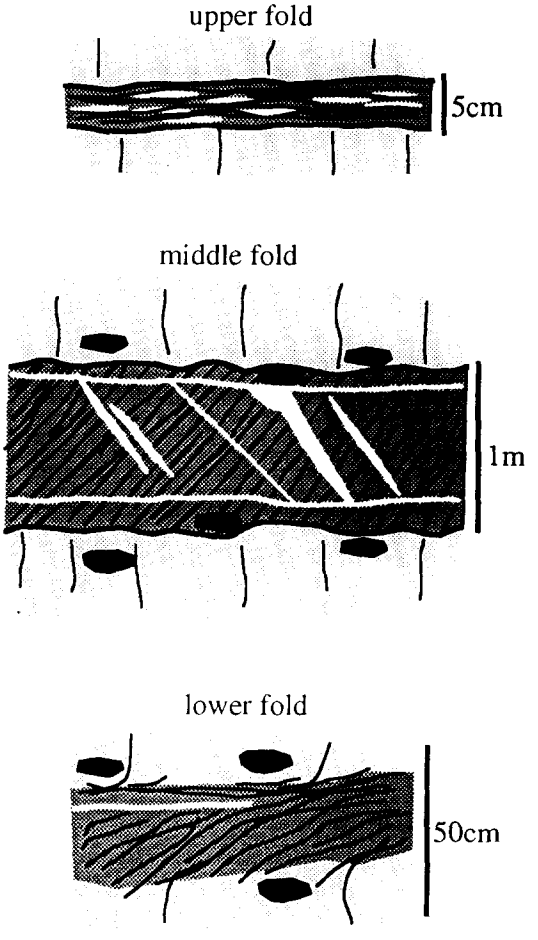

Fig. 7. Sketches of representative bedding-parallel shear zones from the upper, middle and lower folds. Bedding is horizontal, massive layers are shown in light gray, shear zones in dark gray, cleavage traces and chert nodules in black, and calcite veins in white. All sketches correspond to SSW limb orientations. Note that scales are not identical.

sections were viewed towards N20°W (looking into the cross-section).

The orientation and magnitudes of strain increments are conveniently displayed on cumulative incremental strain history (CISH) diagrams, where the horizontal axis is orientation in degrees and the vertical axis represents the cumulative magnitude of incremental elongations. Figure 8 shows how the orientations of horizontal, bedding and cleavage plot relative to the incremental strain history on a CISH diagram for a typical fiber. Clockwise is negative and counterclockwise is positive on CISH diagrams by convention (Beutner & Diegel 1985). The dip direction of N70°E (parallel to the projection of the inferred transport direction), is used as a reference direction for analyses of cleavage-parallel Z sections (Fig. 9). Cleavage was used as a reference direction for all Y section analyses, and thus will always plot at 0° on CISH diagrams (Figs. 8 and 10). A vertical trajectory on a CISH diagram represents straight fibrous overgrowths, a horizontal trajectory represents a kink (rigid rotation of the incremental

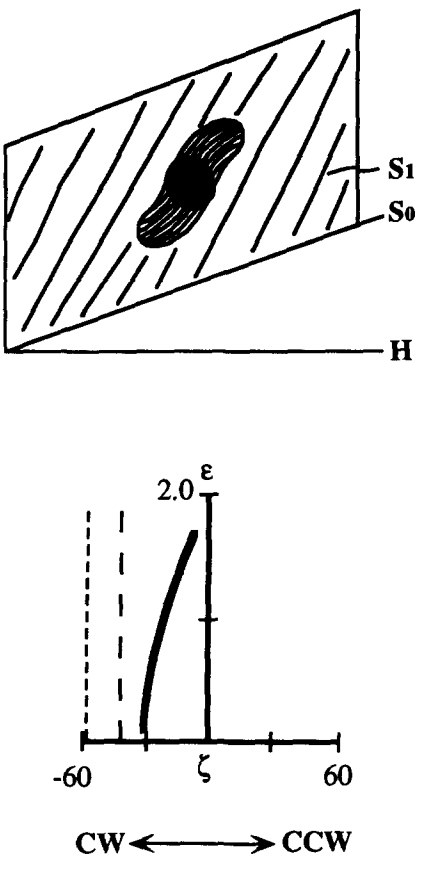

Fig. 8. Sketch showing fibrous overgrowth in a pressure shadow viewed perpendicular to the bedding–cleavage intersection and a representative CISH diagram. Cleavage (S_1) = 0°, bedding (S_0) dashed line, horizontal (H) dotted line.

extension direction relative to the pressure shadow) in the mineral fibers, and a sloping trajectory represents curved fibrous overgrowths. The slope at any point on the curve is inversely proportional to the radius of fiber curvature and reflects the instantaneous vorticity (internal vorticity plus spin). Incremental strain histories for individual fibers are represented as thin grey lines on CISH diagrams. An 'average' incremental strain history

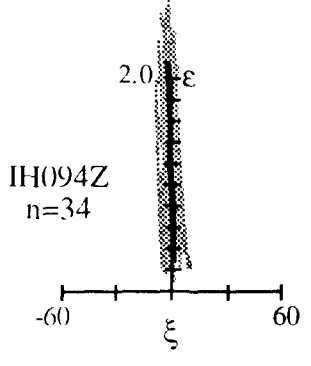

Fig. 9. Cumulative incremental strain history (CISH) diagram for fibers in a cleavage-parallel (Z) section of sample IH094. The inferred transport direction (N70°E) was used as a reference direction and plots at 0° on the CISH diagram. A coaxial strain history in this orientation indicates coaxial down-dip extension and plane-strain deformation. Light curves represent individual fibers and the bold curve represents an average incremental strain history.

for each sample is calculated using the method outlined in Clark *et al.* (1993).

Results

Incremental strain histories reconstructed from fibers in cleavage-parallel (Z) sections are straight and down-dip (Figs. 4b and 9), indicating that deformation was plane strain, with little or no displacement out of the plane of cross-section. Fibers viewed in fold axis-normal (Y) sections are typically curved (Fig. 4a), yielding the CISH diagrams shown in Figs. 10(a) & (b).

Fibers in sample IH162 from the shear zone on the backlimb of the upper fold record a counterclockwise rotation of the incremental elongation direction as strain accumulates, where early increments are nearly bedding-parallel and the latest increments are oriented approximately 20° from bedding. The latest increments of fiber growth are nearly cleavage-parallel in this sample. Antitaxial fibrous extensional veins in a sample from the forelimb of the same shear zone (IH137) show the opposite sense of rotation, with initial increments of extension approximately 60° counterclockwise of bedding and later increments approximately 50° counterclockwise of bedding.

Samples from within shear zones on the backlimb of the middle fold (IH001, IH016, IH022, IH028, IH030, IH034, IH038, IH046, IH127, IH131 and IH150) show counterclockwise rotations of the incremental extension direction, with early fiber increments approaching bedding-parallel and the latest fiber increments inclined at a moderate angle from bedding. The final increment of fiber growth for these samples is often nearly parallel to cleavage. Sample IH012 is located below the upper shear zone and shows a clockwise rotation of the incremental extension direction, with early fiber increments approximately 60° from bedding and the latest increments approximately 25° from bedding. Samples from the shear zone on the forelimb of the middle fold (IH056, IH057, IH072, IH083, IH085 and IH087) show clockwise rotations of the incremental extension direction, with early fiber increments approximately bedding-parallel, and the latest fiber increments at a steeper angle from bedding. As with samples from the backlimb, late fiber increments are close to cleavage-parallel. Sample IH069 is located immediately above the shear zone on the forelimb of the upper fold and shows a counterclockwise rotation of the incremental extension direction, with early fiber increments approximately 60° from bedding and the latest increments approximately 20° from bedding.

Shear zone samples from the backlimb of the lower fold (IH115, IH116, IH118 and IH119) show a counterclockwise rotation of the incremental extension direction relative to the host grain, with early fiber increments nearly bedding-parallel and the latest increments at 30–45° from bedding (Fig. 10a). Sample IH157, located near the axial surface of this fold, has fibers that record nearly coaxial elongation at an orientation 20° clockwise from bedding. Samples IH111, IH113, IH168, IH169 and

IH170 from the forelimb of the lower fold contain fibers that record a clockwise rotation of the incremental extension direction relative to the host grain. Late fiber increments are nearly cleavage parallel for samples from the backlimb of the lower fold, and range from cleavage-parallel to clockwise of cleavage for forelimb samples. Thus fibers in shear zone samples from all three folds record a reversal of fiber curvature near the fold hinge. Fibers in samples from outside of the shear zones curve the opposite sense from shear zone fibers on the same limb.

Finite elongations measured from fibrous overgrowths commonly range from 1.0 to 2.5, and are as high as 3.5 in some samples. Curved fibers in Y sections record relative reorientations of the incremental strain direction of up to 45°, most commonly between 20° and 30° (Figs. 10a & b).

Interpretation

Curved mineral fibers indicate a rotation of the incremental extension direction relative to the porphyroclast, and are typically interpreted as resulting from either: (1) rotation of the sample through a spatially fixed incremental extension direction (spin); or (2) progressive rotation of fiber increments relative to the porphyroclast during non-coaxial strain (internal vorticity) (Beutner & Diegel 1985, Means 1994). In ideal bedding-parallel simple shear, the incremental extension direction is fixed at 45° from bedding such that fibers grow at this orientation and are progressively rotated towards parallelism with bedding as shear accumulates. In samples from the bedding-parallel shear zones at Doublespring, late fiber increments are generally oriented at a moderate angle from bedding (25–55°), with earlier fiber increments progressively closer to parallel with bedding. This pattern of incremental strain histories is interpreted to be compatible with bedding-parallel shear. This interpretation is in agreement with textural evidence such as fabric orientation and en échelon vein arrays which also suggest bedding-parallel shear. Fibers in sample IH137 record primarily bedding-normal extension with a small amount of clockwise rotation of the incremental extension direction. Subparallel cleavage and bedding and the bedding-normal extensional veins are interpreted to be local effects caused by relatively high-amplitude asperities in the shear zone boundary surfaces which would result in small amounts of bedding-normal shortening and extension if shear displacement occurred. This effect is likely only observed in the upper shear zone because the amplitude of the asperities relative to the shear zone thickness is larger in this shear zone. If the fiber curvature is interpreted as a consequence of shear displacement, it is consistent with top toward the hinge shear. Thus the shear sense recorded on each limb of all three folds is consistently top toward the hinge, compatible with flexural-flow towards a pin line located near the axial surface.

Pressure solution cleavage in the shear zones is defined by the concentration of relatively insoluble components in distinct domains or selvages, and thus once formed would have rotated passively with subsequent shear. Comparison of the relative orientations of cleavage, fiber increments and bedding thus allows determination of the timing of cleavage formation and shear relative to the recorded strain history. A nearly cleavage-parallel orientation of the latest increments of fiber growth for samples from the middle and lower shear zones indicates that cleavage developed relatively late in the strain history. Cleavage orientations shallower than 45° to bedding suggest subsequent simple or subsimple shear after cleavage development. Fibers in the extensional veins in sample IH137 are oriented at a high angle to cleavage and are interpreted to largely post-date cleavage formation.

The kinematics within massive layers between bedding-parallel shear zones is less well constrained, as only two (<5%) samples collected from these layers contain incremental strain indicators. Both of the samples from these layers (Fig. 10b) containing fibrous overgrowths (IH012 and IH069) are located adjacent to bedding parallel shear zones (within 5 cm), in narrow, local zones of intermediate fabric intensity. The early extension increments oriented at a high angle from bedding and later increments at a moderate to shallow angle from bedding recorded in these samples are not compatible with bedding parallel shear, and may instead reflect spin through spatially fixed, steep (~70°), diverging extension directions. More data are required to adequately constrain the kinematics of these layers.

DISCUSSION

Relative timing of folding and faulting

The relative timing of folding and faulting is of fundamental importance in the kinematic evolution of fault-related folds, and is often ambiguous in natural structures (Dahlstrom 1970). Several observations suggest that the propagation of imbricate faults preceded folding in the Doublespring duplex. Because of the curved nature of the folds in the Doublespring duplex, footwall synclines would be expected if folding preceded faulting. The lack of a footwall syncline near the trailing edge of the horse (footwall for upper fold) thus suggests that faulting occurred before folding. Morphological differences (thickness, fabric orientation and distribution) between bedding-parallel shear zones in each of the folds suggest that they did not form as a single, continuous shear zone, but were likely structurally isolated when they developed. Because shear zone development is interpreted to be coincident with folding, this suggests that the thrust ramps formed prior to folding.

This conclusion is intuitively satisfying because failure criteria for elastic fracturing and viscous buckling predict that massive (thick) layers are more likely to fail by faulting than buckling under similar physical conditions. The faulting instability envelope (Drucker & Prager

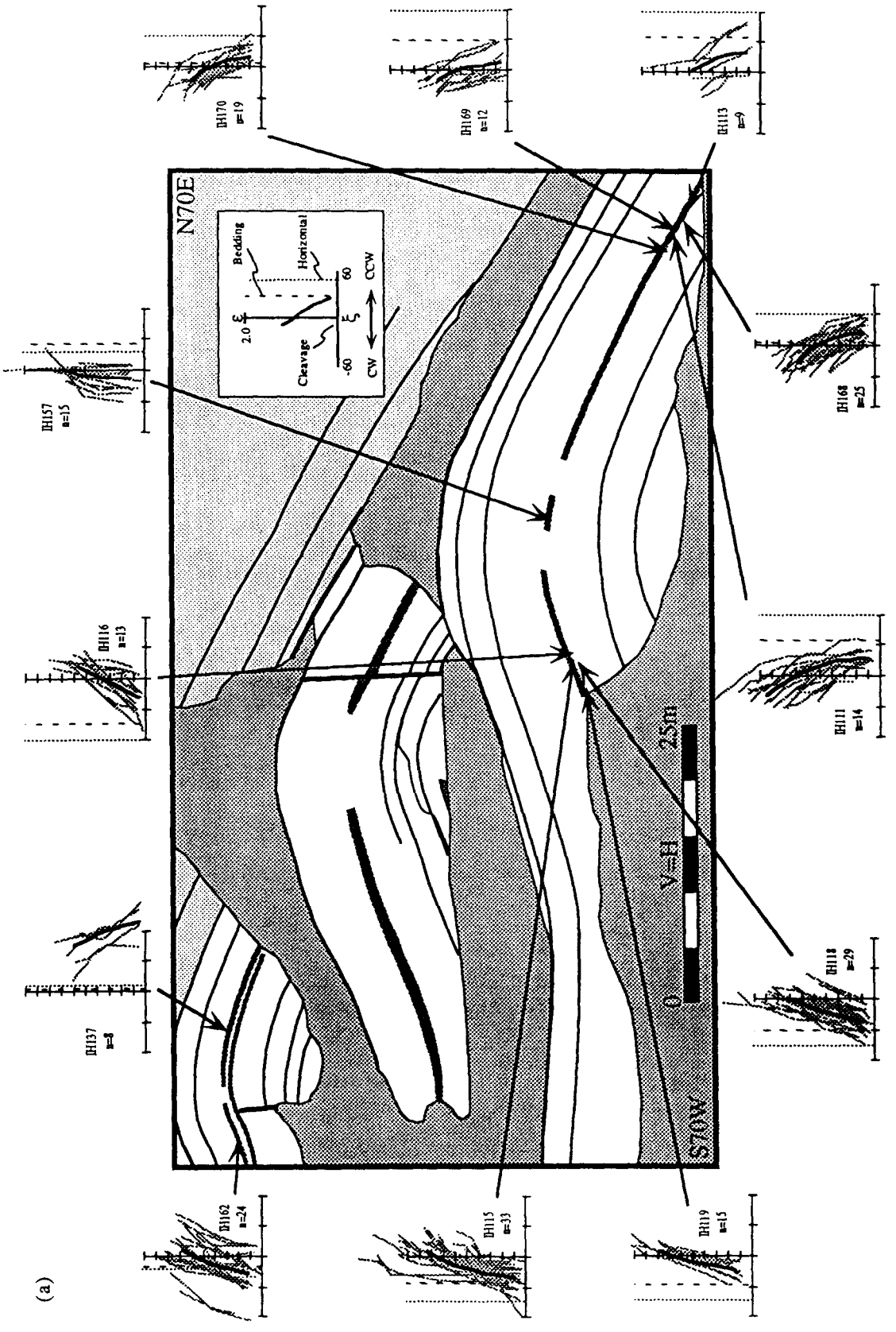
N70E
S70W
V=H
25m
0
Bedding
Horizontal
Cleavage
2.0
60
-60
CCW
CW
DH170 n=19
DH169 n=12
DH113 n=9
DH157 n=15
DH168 n=25
DH116 n=13
DH111 n=14
DH137 n=8
DH118 n=29
DH162 n=24
DH115 n=33
DH119 n=15
(a)

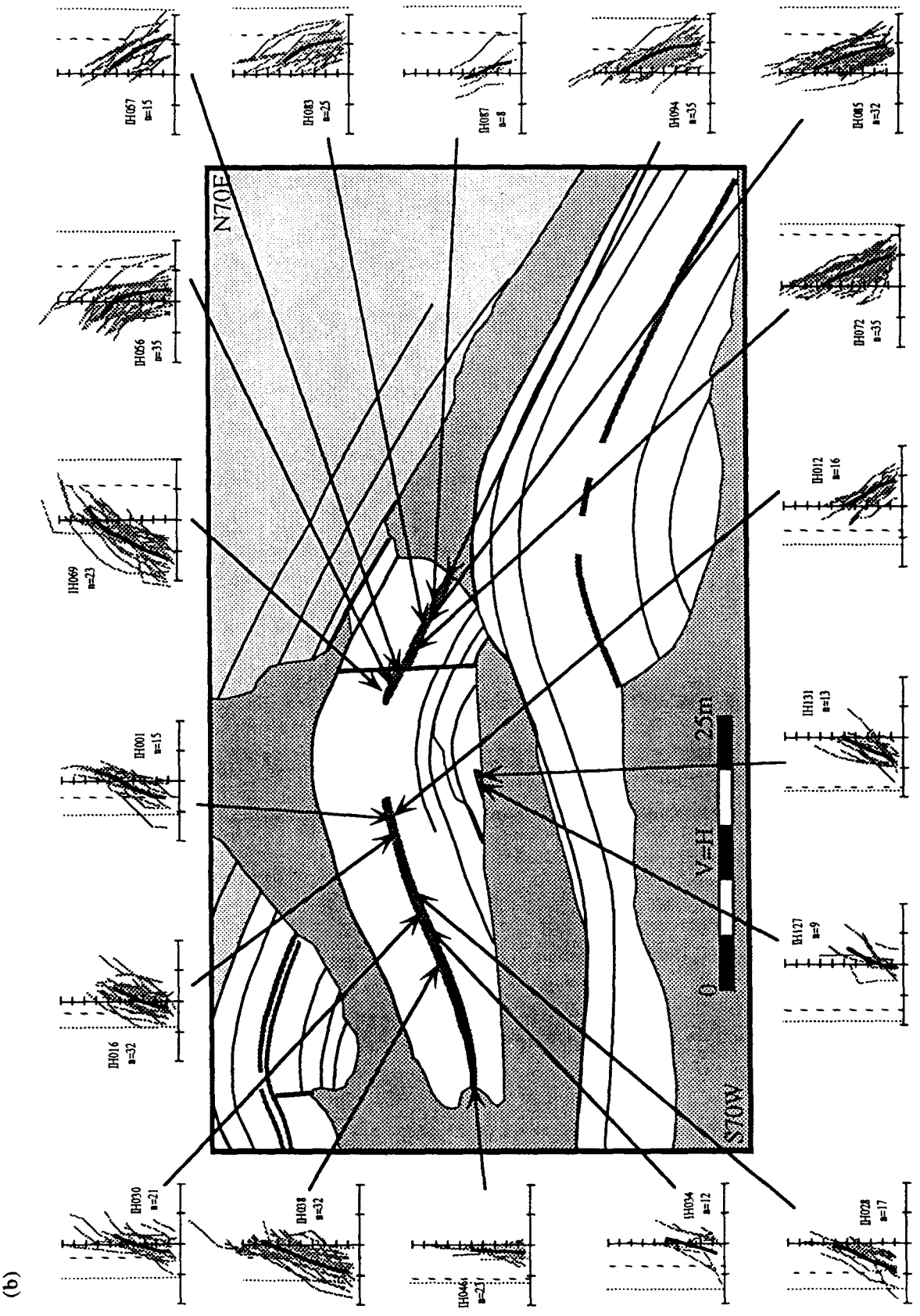

Fig. 10. Detailed sketch of folds in the Doublespring duplex in their present orientation (see Figs. 3 and 5 for location). Beds are shaded as in Fig. 5, shear zones are shown in dark gray, and covered intervals are shown in medium gray. CISH diagrams are shown for fold axis-normal (Y) sections, with arrows indicating sample locations. (a) Incremental strain data from the upper and lower folds. (b) Incremental strain data from the middle fold. Scale and orientation conventions for CISH diagrams as illustrated in upper right of (a). Cleavage = 0°, dashed line represents bedding, and dotted line represents horizontal. Light curves represent individual fibers and the bold curve represents an average incremental strain history.

1952, Jamison 1992) is independent of layer thickness, but the critical stress for viscous buckling varies with the cube of layer thickness (Ramberg 1960, 1961) and thus would be relatively high for the thick, massive beds of the Scott Peak Formation. Thus folds in the Doublespring duplex are fundamentally different from folds that are interpreted to have formed by buckling before (Fischer *et al.* 1992) or during faulting (Fisher & Anastasio 1994).

Kinematics of folding

When taken as an evolutionary sequence where the upper fold represents an early stage with little displacement and an axial surface fixed near the upper footwall cutoff and the middle fold represents a later stage with greater displacement and an axial surface fixed at the lower hanging wall cutoff, the fold geometries and axial surface relationships are suggestive of fault-bend folding with migrating axial surfaces (e.g. Sanderson 1982, Suppe 1983). Shallow bed cutoff angles, open interlimb angles, and a fault-before-fold sequence of deformation are also consistent with a fault-bend fold origin for folds in the Doublespring duplex. The variation in spacing of and displacement on imbricates within the Doublespring duplex allow examination of folds related to different types of axial surfaces at various stages of development. Kinematic models of parallel fault-bend folding (Sanderson 1982, Suppe 1983) predict specific senses and magnitudes of simple shear to occur at different times and locations through the evolution of the fold, including a shear reversal at the top of the footwall ramp (Fig. 1). The observed incremental strain histories from folds in the Doublespring duplex are not compatible with these predictions, but instead consistently record bedding-parallel shear towards pins located at fold axial surfaces regardless of the amount of translation the thrust sheet has experienced. This suggests that either: (1) not all of the shear events associated with fault-bend folding are recorded; or (2) the observed incremental strain histories and associated fabrics are not a consequence of fault-bend folding. Because folding at each of the axial surfaces presumably occurred under similar physical conditions, it is unlikely that only selective events would be recorded. This suggests that the observed incremental strain histories are indeed reflective of folding about a fixed-hinge.

Recent studies have interpreted other asymmetric fault-related folds to have formed by buckling about a fixed hinge based on the distribution of structural fabrics (Fischer *et al.* 1992) and incremental strain histories (Fisher & Anastasio 1994). Folds in the Doublespring duplex are fundamentally different from these structures in that they are interpreted to have formed after thrust-ramp propagation. Theoretical considerations suggest that resistance to bending of a thrust sheet is an important impediment to translation over a thrust ramp (e.g. Wiltchko 1979). A fault-before-fold sequence suggests that the incremental strain history recorded by fibers in the shear zones at Doublespring occurred during fixed-hinge buckle folding in response to resistance to initial translation of the thrust sheet up the ramp. Leading edge antithetic faulting in the upper and middle folds of the Doublespring duplex also likely occurred in response to resistance to bending at the base of the thrust ramps (e.g. Serra 1977).

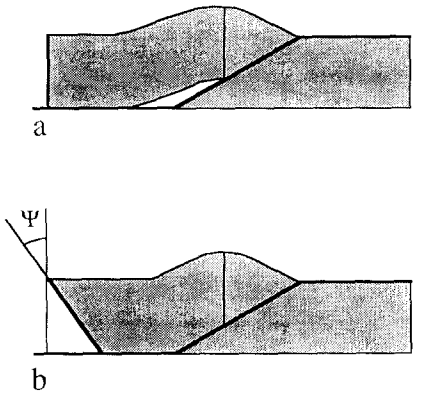

Fig. 11. (a) Volume problem associated with fixed-hinge buckle folding. Excess cross-sectional area must be accommodated by mass transfer or brecciation, or supported as an open void. (b) Top-to-the-hinterland shear in the thrust sheet required to preserve shallow hanging wall cutoffs and open interlimb angle during fixed-hinge buckling. Steeper hanging wall cutoffs and a tight interlimb angle are required to eliminate shear in the thrust sheet.

Fixed-hinge folding on the ramp to the present amplitudes and interlimb angles would have required either ductile flow in the hinge area (Fig. 11a), or top-to-the-hinterland shear in the thrust sheet (Fig. 11b) to accommodate the volume problem in the hinge and preserve shallow hanging wall cutoffs. Fixed-hinge folding creates a volume problem in the core of the fold that must be accommodated by ductile flow in the décollement or supported as an open volume (e.g. Laubscher 1976, Fischer *et al.* 1992). Although there is no ductile unit above the décollement in the Doublespring duplex, some thickening in the unexposed core of the middle fold is apparent (Figs. 3 and 10). Because this fold has been completely translated onto the upper flat, this apparent thickening could have resulted from either buckling on the ramp or from subsequent folding at the top of the ramp. Top-to-the-hinterland shear accommodating folding is unlikely since shear zones are restricted to the limbs of anticlinal folds, suggesting that no shear unrelated to folding has occurred, and implying a nearly vertical trailing edge loose line for the thrust sheet. After the folds formed as fixed-hinge buckle folds, they were later modified due to fault-bend folding with subsequent translation of the thrust sheets. The magnitude of the volume problem in the core of the folds would have been relatively small if the folds initially formed with low amplitudes and gentle to open interlimb angles and were later tightened as they were translated over the ramp.

Evolution of folds in the Doublespring duplex

Structural geometries, tectonic fabric distributions and incremental strain histories suggest an evolutionary history for fault-related folds in the Doublespring

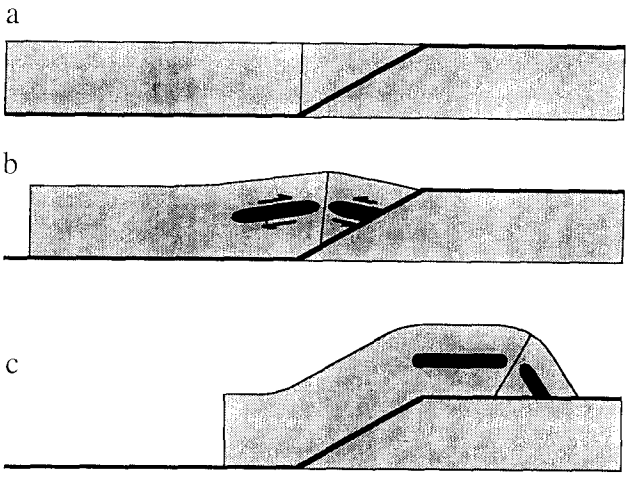

Fig. 12. Kinematic evolution of fault-related folds in the Doublespring duplex. (a) Propagation of thrust fault. (b) Low-amplitude fixed-hinge buckling and bedding-parallel shear zone development occurs in response to resistance to translation up the ramp. (c) Subsequent translation modifies fold geometry to approximate fault-bend fold geometry.

duplex as follows. The structures originated when the imbricate thrust ramp formed in response to a fracture instability (Fig. 12a). Increased stress caused by resistance to translation on the stepped fault surface caused low amplitude buckling of the thrust sheet and development of bedding-parallel shear zones (Fig. 12b). Fiber growth was contemporaneous with shear zone development, and it is this event that is recorded in the incremental strain histories. Because the pressure solution strain rate is known to be proportional to deviatoric stress (Rutter 1976), the effectiveness of pressure solution as a deformation mechanism would have been enhanced during this period of elevated stress magnitudes. Low-amplitude buckling may have occurred at axial surfaces located on a ramp (upper fold), at the base of a ramp (middle fold), or away from a ramp (lower fold?) (Fig. 5). After the initial resistance to translation was overcome by buckling and shear zone development, thrust sheets were translated to form the present fold geometry by fault-bend folding (Fig. 12c). Despite the fact that additional deformation would have been required to accommodate additional folding, no textural record of translation or fault-bend folding is apparent. This is indicated by the similarity in the kinematics of the three folds despite their different translational histories. For example, no reversal of shear direction has been recorded in the backlimb of the middle fold despite the fact that the horse was completely translated over the top of the footwall ramp and along the upper flat. Thus strain accommodated fault-bend folding occurred by a different mechanism, perhaps because these processes occurred under lower stress conditions. Strain softening caused by shear zone formation and late-stage bedding-parallel faulting may have allowed subsequent deformation to occur with less penetrative strain.

CONCLUSIONS

Analysis of the structural geometry, distribution of tectonic fabrics and incremental strain data from the Doublespring duplex leads to several important conclusions about the structural evolution of fault-related folds in the duplex.

(1) No textural fabric is associated with propagation of faults, translation of the thrust sheet along a flat, or fault-bend folding, while shear zones and fibers in overgrowths and veins record a period of buckle folding. This suggests that the stress conditions may have been different during buckling and fault-bend folding.

(2) Fibers record only the incremental strain history associated with buckle folding, and only in areas affected by mass transfer (i.e. shear zones). Distributions of fabrics and incremental strain histories indicate that different layers experience different kinematic histories associated with folding. These data suggest flexural-flow folding around a pin near the fold hinge occurred in bedding-parallel shear zones, and massive layers experienced rotation through spatially fixed, steep (~70°), diverging extension directions.

(3) Fault-related folds may initiate in response to a fracture instability, like a fault-bend fold, and later experience fixed-hinge buckling in response to resistance to translation.

Acknowledgements—This paper represents a portion of C. A. Hedlund's M.S. thesis at Lehigh University. This research was supported by NSF grants EAR-9017334 to D. J. Anastasio and EAR-9018433 to D. M. Fisher, and by grants from the American Association of Petroleum Geologists, the Geological Society of America, and Sigma Xi to C. A. Hedlund. The authors acknowledge R. W. Allmendinger for use of Stereonet software, V. Johnson for logistical support and W. Means for a preprint of his paper on rotational quantities and the development of small-scale structures. This manuscript has benefitted from discussions with M. A. Krol and M. S. Wilkerson, and from reviews by M. A. Ellis, D. A. Ferrill and J. R. Henderson.

REFERENCES

Baldwin, E. M. 1951. Faulting in the Lost River Range area of Idaho. *Am. J. Sci.* **249**, 884–902.

Beutner, E. C. & Diegel, F. 1985. Determination of fold kinematics from syntectonic fibers in pressure shadows, Martinsburg slate, New Jersey. *Am. J. Sci.* **285**, 15–50.

Beutner, E. C., Fisher, D. M. & Kirkpatrick, J. L. 1988. Kinematics of deformation at a thrust fault ramp (?) from syntectonic fibers in pressure shadows. In: *Geometries and Mechanisms of Thrusting, With Special Reference to the Appalachians* (edited by Mitra, G. & Wojtal, S.). *Spec. Pap. geol. Soc. Am.* **222**, 77–88.

Boyer, S. E. 1986. Styles of folding within thrust sheets: examples from the Appalachians and the Rocky Mountains of the U.S.A. and Canada. *J. Struct. Geol.* **8**, 325–339.

Clark, M. B., Fisher, D. M. & Chia-Yu, L. 1993. Kinematic analysis of the Hfuehshan Range: A large-scale pop-up structure. *Tectonics* **12**, 205–217.

Crone, A. J. & Haller, K. M. 1991. Segmentation and the coseismic behavior of Basin and Range normal faults: examples from east-central Idaho and southwestern Montana, U.S.A. *J. Struct. Geol.* **13**, 151–164.

Dahlstrom, C. D. A. 1970. Structural geology in the eastern margin of

the Canadian Rocky Mountains. *Bull. Can. Petrol. Geol.* **18**, 332–406.

Durney, D. W. & Ramsay, J. G. 1973. Incremental strains measured by syntectonic crystal growth. In: *Gravity and Tectonics* (edited by DeJong, K. A. & Scholten, R.). Wiley, New York, 67–96.

Drucker, D. C. & Prager, W. 1952. Soil mechanics and plastic analysis for limited design. *Q. J. Appl. Math.* **10**, 157–165.

Elliott, D. 1972. Deformation paths in structural geology. *Bull. geol. Soc. Am.* **83**, 2621–2638.

Ellis, M. A. 1986. The determination of progressive deformation histories from antitaxial syntectonic fibers. *J. Struct. Geol.* **8**, 701–709.

Fischer, M. P., Woodward, N. B. & Mitchell, M. M. 1992. The kinematics of break-thrust folds. *J. Struct. Geol.* **14**, 451–460.

Fisher, D. M. 1990. Orientation history and rheology in slates, Kodiak and Afognak Islands, Alaska. *J. Struct. Geol.* **12**, 483–498.

Fisher, D. M. & Byrne, T. 1992. Strain variations in an ancient accretionary complex: Implication for forearc evolution. *Tectonics* **11**, 330–347.

Fisher, D. M. & Anastasio, D. J. 1994. Kinematic analysis of a large-scale leading edge fold, Lost River Range, Idaho. *J. Struct. Geol.* **16**, 337–354.

Geiser, P. A. 1988. The role of kinematics in the construction and analysis of geological cross sections in deformed terranes. In: *Geometries and Mechanisms of Thrusting, With Special Reference to the Appalachians* (edited by Mitra, G. & Wojtal, S.). *Spec. Pap. geol. Soc. Am.* **222**, 47–76.

Jamison, W. R. 1987. Geometric analysis of fold development in overthrust terranes. *J. Struct. Geol.* **9**, 207–219.

Jamison, W. R. 1992. Stress controls on fold thrust style. In: *Thrust Tectonics* (edited by McClay, K. R.). Chapman & Hall, London, 155–164.

Laubscher, H. P. 1976. Fold development in the Jura. *Tectonophysics* **37**, 337–362.

Mamet, B. L., Skipp, B., Sando, W. J. & Mapel, W. J. 1971. Biostratigraphy of Upper Mississippian and associated Carboniferous rocks in south-central Idaho. *Bull. Am. Ass. Petrol. Geol.* **55**, 20–33.

Mapel, W. J., Read, W. H. & Smith, R. K. 1965. Geologic map and sections of the Doublespring quadrangle, Custer and Lemhi Counties, Idaho. *U.S. geol. Surv. Geol. Quad. Map.* **GQ-464**.

Marshak S. & Engelder, T. 1985. Development of cleavage in limestones of a fold–thrust belt in eastern New York. *J. Struct. Geol.* **7**, 345–359.

Means, W. D. 1994. Rotational quantities in homogenous flow and the development of small-scale structure. *J. Struct. Geol.* **16**, 437–445.

Mitra, S. 1990. Fault-propagation folds: Geometry, kinematic evolution, and hydrocarbon traps. *Bull. Am. Ass. Petrol. Geol.* **74**, 921–945.

Mitra, S. 1992. Balanced structural interpretations in fold and thrust belts. In: *Structural Geology of Fold and Thrust Belts* (edited by Mitra, S. & Fisher, G. W.). Johns Hopkins Press, Baltimore.

Ramberg, H. 1960. Relationship between length of arc and thickness of ptygmatically folded veins. *Am. J. Sci.* **258**, 36–46.

Ramberg, H. 1961. Contact strain and folding unstability of a multilayered body under compression. *Geol. Rdsch.* **51**, 405–439.

Ramsay, J. G. 1982. Rock ductility and its influence on the development of tectonic structures in mountain belts. In: *Mountain Building Processes* (edited by Hsü, K. J.). Academic Press, New York.

Ramsay, J. G. & Graham, R. H. 1970. Strain variation in shear belts. *Can. J. Earth Sci.* **7**, 786–813.

Ramsay, J. G. & Huber, M. I. 1983. *The Techniques of Modern Structural Geology, Volume* 1: *Strain Analysis*. Academic Press, New York.

Rich, R. L. 1934. Mechanics of low-angle overthrust faulting as illustrated by Cumberland thrust block, Virginia, Kentucky, and Tennessee. *Bull. Am. Ass. Petrol. Geol.* **18**, 1584–1596.

Rose, P. R. 1977. Mississippian carbonate shelf margins, western United States. *Wyoming geol. Ass., 29th Annual Field Conf. Guidebook*, 155–172.

Ross, C. P. 1947. Geology of the Borah Peak quadrangle, Idaho. *Bull. geol. Soc. Am.* **58**, 1085–1160.

Rutter, E. H. 1976. The kinetics of rock deformation by pressure solution. *Phil. Trans. R. Soc. Lond.* **283**, 203–219.

Sample, J. C. & Fisher, D. M. 1986. Duplex accretion and underplating in an ancient accretionary complex, Kodiak Islands, Alaska. *Geology* **14**, 160–163.

Sanderson, D. J. 1982. Models of strain variation in nappes and thrust sheets: a review. *Tectonophysics* **88**, 201–233.

Serra, S. 1977. Styles of deformation in the ramp regions of overthrusts faults. *Wyoming geol. Ass., 29th Annual Field Conf. Guidebook*, 487–498.

Skipp, B., Sando, W. J. & Hall, W. E. 1979. The Mississippian and Pennsylvanian (Carboniferous) Systems in the United States—Idaho. *Prof. Pap. U.S. geol. Surv.* **1110-AA**.

Suppe, J. 1983. Geometry and kinematics of fault-bend folding. *Am. J. Sci.* **283**, 648–721.

Suppe, J. & Medwedeff, D. A. 1984. Fault-propagation folding. *Geol. Soc. Am. Abs. w. Prog.* **16**, 670.

Suppe, J. & Medwedeff, D. A. 1990. Geometry and kinematics of fault-propagation folding. *Eclog. geol. Helv.* **83**, 409–454.

Wickham, J. S. 1973. An estimate of strain increments in a naturally deformed carbonate rock. *Am. J. Sci.* **273**, 23–47.

Wickham, J. & Anthony, M. 1977. Strain paths and folding of carbonate rocks near Blue Ridge, central Appalachians. *Bull. geol. Soc. Am.* **88**, 920–924.

Willis, B. 1893. Mechanics of Appalachian structure. *U.S. geol. Surv. Annual Rep.* 13 (1891–1892), Part 2, 217–281.

Wiltschko, D. V. 1979. Mechanical model for thrust sheet deformation at a ramp. *J. geophys. Res.* **84**, 1091–1104.

Woodward, N. B., Boyer, S. E. & Suppe, J. 1989. Balanced geological cross-sections: An essential technique in geological research and exploration. *Am. Geophys. Un. Int. Geol. Conf. Short Course in Geology* **6**.